energies

MDPI

Article

Effect of Radio-Frequency Power on the Composition of $BiVO_4$ Thin-Film Photoanodes Sputtered from a Single Target

Jiaqi Liu [1,*], Kazuya Tajima [1], Imane Abdellaoui [1], Muhammad Monirul Islam [1,2], Shigeru Ikeda [3] and Takeaki Sakurai [1,*]

[1] Institute of Applied Physics, University of Tsukuba, Tsukuba 305-8573, Ibaraki, Japan; s1920325@s.tsukuba.ac.jp (K.T.); s1830099@s.tsukuba.ac.jp (I.A.); islam.monir.ke@u.tsukuba.ac.jp (M.M.I.)
[2] Alliance for Research on the Mediterranean and North Africa (ARENA), University of Tsukuba, Tsukuba 305-8573, Ibaraki, Japan
[3] Department of Chemistry, Konan University, Kobe 658-8501, Hyogo, Japan; s-ikeda@konan-u.ac.jp
* Correspondence: s1936008@s.tsukuba.ac.jp (J.L.); sakurai@bk.tsukuba.ac.jp (T.S.)

Abstract: $BiVO_4$ films were fabricated by radio frequency (RF) sputtering from a single target. The deposited $BiVO_4$ films were found to be rich in Bi, and the reason for the Bi-richness was investigated. It was inferred from the Monte Carlo simulation that, during sputtering, the transfer process of target atoms through argon gas played a major role in this phenomenon. The transfer process resulted in an imbalanced ratio of Bi and V, arising from the difference in atom mass and interaction radius. The high RF power was found to be effective in adjusting the Bi/V ratio, influencing the sputtering yield. This type of preferential sputtering was maintained by the diffusion of target atoms from the bulk to the surface. $BiVO_4$ films with monoclinic scheelite crystal structures were obtained at high RF power values and found to exhibit photocatalytic performances beneficial for photoanodic applications.

Keywords: photocatalyst; bismuth vanadate films; RF sputtering; compound target

Citation: Liu, J.; Tajima, K.; Abdellaoui, I.; Islam, M.M.; Ikeda, S.; Sakurai, T. Effect of Radio-Frequency Power on the Composition of $BiVO_4$ Thin-Film Photoanodes Sputtered from a Single Target. *Energies* **2021**, *14*, 2122. https://doi.org/10.3390/en14082122

Academic Editor: Dipali S. Patil

Received: 7 February 2021
Accepted: 7 April 2021
Published: 10 April 2021

1. Introduction

Solar energy, as a sustainable resource, has enormous potential in future energy systems. Due to its intermittency, harvesting and storage strategies must be efficient to implement. Water splitting is a promising technique for converting solar energy to hydrogen [1]. Regarding water splitting, water oxidation conditions require the stability of the anode materials under illumination. Bismuth vanadate ($BiVO_4$) has emerged as the most interesting among the thermodynamically stable metal oxides because of its essence [2]. A bandgap of approximately 2.4 eV in the monoclinic phase (which has been confirmed as the best phase of $BiVO_4$ for photocatalysis [3]) ensures sufficient sunlight harvest [4]. The valence band edge of $BiVO_4$ is lower than the water oxidation potential (1.23 V vs. normal hydrogen electrode (NHE) at pH 0), suggesting that $BiVO_4$ is capable of generating O_2 from water thermodynamically [5]. These merits have contributed to the rapid development of $BiVO_4$ as a photoanode material in recent years. An incident photon-to-current efficiency of ~90% has been achieved by using WO_3, which is more conductive to the formation of a heterojunction that promotes carrier diffusion [6].

Given its rapid development as a photocatalytic anode material, $BiVO_4$ has recently attracted attention in the field of supercapacitors. When $BiVO_4$ was first utilized as the anode material in lithium–ion capacitors, the energy and power densities obtained met the power demands of the Partnership for a New Generation of Vehicles (PNGV) research program [7]. In this fascinating field of energy, the development of fabrication methods is essential to accelerate industrialization.

There are several methods that are developed for fabricating $BiVO_4$ films [8,9], which are prevalent, owing to their stability in solutions compared with other configurations (such as powder). Different methods determine the properties of materials, such as the

state of defects and overall conductivity and its type, as well as the possibility of practical applications [10,11]. Sputtering can be considered as a scalable deposition method for solar-driven fuel production on a large scale because it has been extensively used in industries [12]. In addition, the growth environment of the film in a vacuum is beneficial to film quality. Sputtering has extensively been adopted on $BiVO_4$ films in recent years; the co-sputtering technique has proven to be the most superior method, owing to the lopsided element ratio in the sputtered films of the single-compound $BiVO_4$ target [13,14]. This kind of imbalanced element ratio was also found in a later study [15], which resulted in excess bismuth in the prepared films, and, in turn, limited the photocatalytic performance. Sputtering from a single target can reduce the tedious steps and additional expenditure on equipment. Therefore, the key to realizing single-target sputtering on $BiVO_4$ is to control the ratio balance of the sputtered films.

In this work, the sputtering process of a compound target was specifically analyzed, and the predominant factors affecting the element ratio of films were discussed. Moreover, different radio frequency (RF) powers were applied to the single $BiVO_4$ target to form the films. The structures and photocatalytic performances of the prepared films were investigated to demonstrate the feasibility of fabricating monoclinic scheelite $BiVO_4$ films by sputtering from a single target.

2. Materials and Methods

2.1. Deposition of $BiVO_4$ Films

All the films were deposited with a compound $BiVO_4$ target (Φ60 mm, Toshima Manufacturing, Saitama, Japan) on alkaline earth boro-aluminosilicate glass (Eagle XG, Corning) and fluorine-doped tin oxide (FTO, TEC7, Sigma-Aldrich: Louis, MO, USA) glass substrates. The substrates were cleaned ultrasonically with acetone and methanol (each for 10 min, twice), followed by ultrasonic cleaning in deionized water for 10 min, and finally dried by nitrogen purging before loading into the sputtering chamber. The $BiVO_4$ thin films were deposited at room temperature (20 °C) and different RF powers (50 W, 120 W, and 200 W). Argon gas was used to produce an argon plasma environment with a pressure of 0.7 Pa, and the deposition time was fixed as 1 h for each case. The substrate was coaxially aligned to the $BiVO_4$ target with a distance of 10 cm between them. After the deposition, all the $BiVO_4$ samples were annealed in a gold-coated tubular furnace at 400 °C for 2 h under an oxygen atmosphere (1 atm.), considering the vanadium (V) loss from the $BiVO_4$ lattice above 450 °C during the annealing with oxygen [16].

2.2. Characterization

The deposited $BiVO_4$ films were characterized via X-ray photoelectron spectroscopy (XPS, JPS-9010series, JEOL). For XPS measurements, narrow scans for all samples were obtained using a pass-energy of 10 eV and a step size of 0.1 eV. A non-monochromatic Mg Kα X-ray source with a centroid photon energy of 1253.6 eV was used for all measurements. The thickness of the films was measured using a mechanical probe profilometer (Surfcom 1500SD-12, Accretech: Hachioji, Tokyo, Japan). The simulation of the transport process was performed using a computational model based on Monte Carlo simulation [17]. The simulation parameters were set based on the practical sputtering environment. The bulk crystalline structures of the prepared films were characterized via X-ray diffraction (XRD, X'pert, Malvern PANalytical) in the θ–2θ mode with Cu Kα radiation (λ = 1.541837 Å), and the voltage and current were set at 45 kV and 40 mA, respectively. The XRD patterns were recorded at room temperature in the 14–60° range with a step size of 0.016746°. Structural analysis was carried out using Rietveld refinement with the FullProf Suite software, and the crystallographic information file (CIF) of monoclinic scheelite $BiVO_4$ was obtained from the Crystallographic Open Database. The morphology of the films was characterized using an JXA-8530F Field Emission Electron Probe Microanalyzer with a scanning electron microscope (SEM) attachment. Photoelectrochemical (PEC) measurements were conducted in an electrolytic solution containing hole scavengers (0.02 mol L^{-1} Na_2S and 0.02 mol L^{-1}

Na_2SO_3) using a conventional three-electrode setup. A Pt wire and a Ag/AgCl electrode were used as the counter and reference electrodes, respectively. Potential sweeps were performed using a potentiostat (Hokuto Denko HSV-110). A solar simulator (Asahi Spectra HAL320) producing AM 1.5G simulated sunlight was used for illumination.

3. Results and Discussion

3.1. Film Composition

Figure 1a shows the element ratio of Bi and V along with the thickness values of the $BiVO_4$ films sputtered at various RF powers. As seen from the figure, the thicknesses of the sputtered films were significantly affected by the RF power, making films with thicknesses in the range of 85–1000 nm, where the thickness increased with an increase in RF power. In terms of the element ratio in films, the relative sensitivity factor (Bi: V ≈ 2.3) provided by the XPS machine was used to calculate it; it was found that excess Bi was produced. Interestingly, the element ratio seemed to be higher when compared with the XRD results of the films (later part). It was also reported in [13] that Bi may tend to migrate to the surface of the films because of high volatility. However, this ratio variation still represented the ratio in bulk as the RF power increases. The observed film composition was related to the entire sputtering process, including the sputtering yield of the constituent atoms in the target, their transport process during sputtering, and the adsorption properties of the target atoms on the substrate. These aspects will be discussed in detail later. In addition, the chemical states of the elements characterized by XPS are shown in Figure 1b,c, and Bi and V were in the single chemical states Bi^{3+} and V^{5+}, respectively.

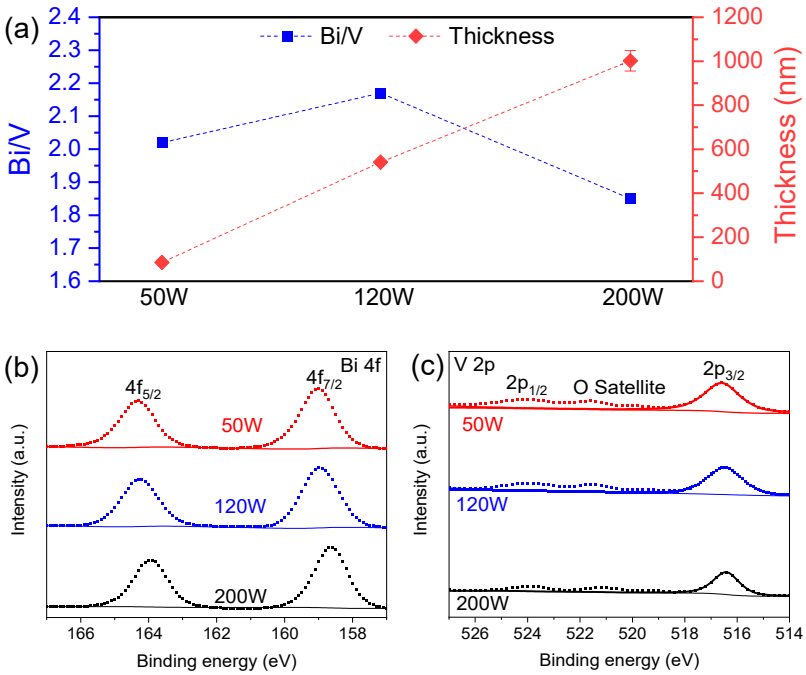

Figure 1. (**a**) Element ratio of Bi and V calculated from the XPS peak area and the thickness of films prepared at various RF powers. Narrow scan X-ray photoelectron spectra in the (**b**) Bi 4f and (**c**) V 2p core-level regions from sputtered bismuth vanadate ($BiVO_4$) thin films with various RF powers. Oxygen satellite peaks in (**c**) were caused by $K\alpha_3$ and $K\alpha_4$ transitions from the non-monochromatic Mg X-ray source [18].

3.2. Monte Carlo Simulation

According to the principle of sputtering, the deposition pressure should be sufficient to obtain a plasma glow. Thus, the mutual effect between the sputtered atoms and background gas cannot be neglected. First, during sputtering, the transportation process of the constituent atoms of the compound target towards the substrate was investigated. In this

process, the main step was the collision between the background gas and the sputtered atoms, which led to a change in the energy and momentum of the sputtered atoms. The number of Bi and V atoms arriving at the substrate was simulated, as shown in Figure 2. The simulated plot indicates that most of the constituent atoms detached from the substrate due to multiple collisions, resulting in only approximately 3100 Bi atoms and 2000 V atoms being able to reach the substrate. Notably, more Bi atoms could reach the substrate, which can be attributed to the interaction between the sputtered atoms and background gas. Although the collision probability of Bi atoms was higher than that of V atoms owing to the stronger interatomic potential of Bi–Ar [19], the residual amount of Bi was more than that of V. The key to this imbalanced ratio can be attributed only to the atomic mass because of two aspects: (1) the change in direction after collision–the greater the mass of the sputtered atom is with respect to that of the background atom, the smaller the angle of change; and (2) the energy loss of the sputtered atoms after collision–the closer the mass of the sputtered atom is to that of the background atom, the greater the energy loss. The higher mass of V atoms thus played a major role in deciding its trajectory deviation and rapid energy loss in the collisions. Note that RF power had approximately no influence on the transport process because of the minor effect of voltage drops (50 W:98 V, 120 W:147 V, 200 W:181 V) on collision.

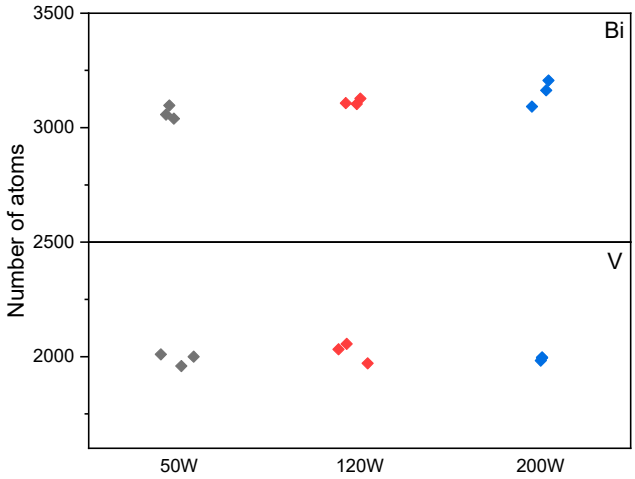

Figure 2. Simulated number of different atoms that can reach the substrate from 10,000 atoms sputtered under various RF powers. The simulation was performed thrice for each case.

3.3. Sputtering Yield

To further explain the significant change in the element ratio of the films, we considered the effect of the sputtering yields of the constituent atoms of the compound $BiVO_4$ target. With respect to the compound target, a surface alteration layer (the thickness is determined by the penetration depth of argon ions) [20,21] can be formed during the sputtering process, which is different in composition compared to the bulk [22]. In this study, for $BiVO_4$ films, excess V was found at the surface of the sputtered films (Figure S1), which can be attributed to the difference in the sputtering yield of each element [23]. The composition of the surface layer of the compound target continued to change until a steady state had been established. For simplicity, we considered only two elements in the target. The density in the bulk of the target was V_0 and Bi_0 atoms/cm^3, and V and Bi represented the density at the surface region at the steady state. At the balance, the following equation should be satisfied related to the substance at the surface layer:

$$\left(\frac{V}{V+Bi}S_V + \frac{Bi}{V+Bi}S_{Bi}\right) \times j = D_{Bi} + (V_0 + Bi_0) \times f, \quad (1)$$

where j is the argon ion current density, and S_V and S_{Bi} represent the sputtering yields of the two elements, respectively. D_{Bi} is the diffusion rate of bismuth from the bulk to the surface

layer (where the diffusion of V is neglected because the diffusion of Bi is predominant). Moreover, f is the transformation frequency of atoms from the bulk to the surface layer. An illustration of the target surface is shown in Figure 3.

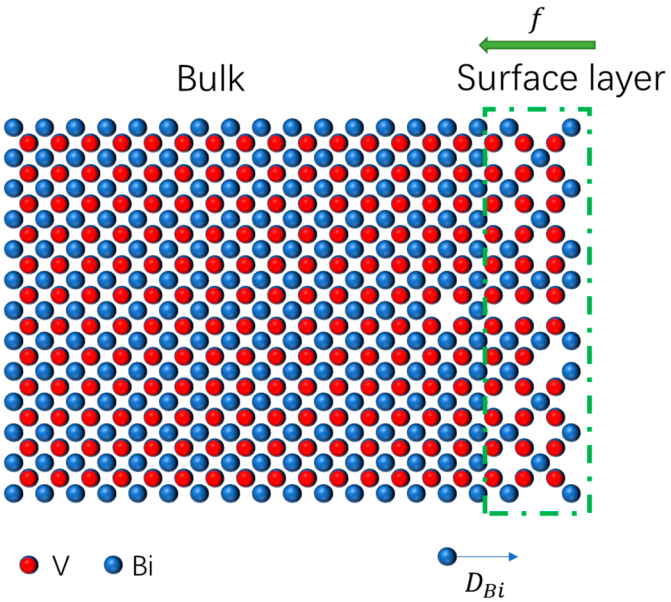

Figure 3. Illustration describing the state of the target surface.

If the diffusion process is neglected, the sputtered ratio is approximately similar to the target composition [24]. Diffusion occurs when the concentration difference is formed with a certain temperature as the driving force. The instant diffusion of Bi atoms from the bulk to the surface was observed at 400 °C in a vacuum (Figure S2) because of the lower Bi content in the surface layer. During sputtering, even if the target is consistently cooled by the circulating water, the target surface maintains a certain high temperature caused by the plasma impact. In this condition, the relative rate (sputtering vs. diffusion) determines the ratio of sputtered atoms. When the sputtering rate is considerably higher than the diffusion rate, similar to when there is no diffusion, the sputtered ratio is close to the target. According to the relationship between the current density and voltage drop [25],

$$j \propto V^{7/2}. \quad (2)$$

The argon ion current density at 200 W RF power should be considerably higher than that at 50 W in agreement with the difference in film thickness. This indicates that the increase in sputtering yield played a dominant role when high power was used, compared with the increased diffusion rate resulting from the increase in the target temperature. Therefore, it is evident that RF power influences the sputtered element ratio, and higher power is beneficial for maintaining the original ratio within the target. However, note that the target composition will change slightly because of diffusion. Therefore, more attention should be drawn to the long-term stability tolerance of the compound target. On the other hand, the sputtered ratio should also be close to the target ratio at very low power because the diffusion rate may slow down in this case. This explains the decrease in the ratio at 50 W below that at 120 W.

3.4. Adsorption on the Substrate

In addition, the number of adsorbed atoms on the substrate can be described as [26]

$$N = Is\tau, \quad (3)$$

where I is the incident number of target atoms at the unit surface per unit time, s is the sticking coefficient, and τ is the average residence time of atoms on the surface. Therein, the sticking coefficient is a function determined by the surface coverage $f(\theta)$, temperature, and activation energy of adsorption E_a:

$$s = f(\theta)e^{\frac{-E_a}{RT}}, \tag{4}$$

where R is the universal gas constant. In terms of time τ, it can be obtained by the Frenkel equation

$$\tau = \tau_0 e^{\frac{E_d}{RT}}, \tag{5}$$

where τ_0 is the preexponential factor and E_d is the activation energy of desorption. To substitute Equations (4) and (5) into Equation (3), N can then be expressed as

$$N = If(\theta)\tau_0 e^{\frac{E_d - E_a}{RT}}. \tag{6}$$

Here, $E_d - E_a$ is equal to the heat of chemisorption, which can be treated as the heat of sublimation. For this case, the difference in N between Bi and V is the focus. Due to the complexity of these parameters, the accurate solution is not discussed here. However, the relationship between N and T could be understood to some extent. The $f(\theta)$ remains the same for two atoms, and τ_0 is proportional to T^{-1} [27]. Therefore, the important impact term is the exponential term of temperature. The heat of sublimation for Bi and V is 2.163 and 5.362 eV/atom, respectively [23]. This means that the adsorbed Bi atoms on the substrate dramatically drop with increasing temperature compared to V atoms. This phenomenon was verified by the films sputtered at various substrate temperatures (Figure S3). As for the effect of RF power on the substrate temperature, it is clear that the incident atoms yield energy to the substrate, occurring mainly in exothermic adsorption. Owing to the large number of atoms impinging on the substrate, the temperature increases, and a slightly higher concentration of V is found in the film resulting from high power, as reported by Kölbach et al. [28].

3.5. Structure and Morphology

The influence of RF power on the crystal structure of $BiVO_4$ films was characterized by XRD. Figure 4a shows the results of the prepared $BiVO_4$ films on glass substrates. All the films exhibit characteristics (reflection (002) at around 15.1°) resembling those of monoclinic scheelite $BiVO_4$. However, for the films fabricated at 50 and 120 W, the impurity phase appears, which could be attributed to the high Bi concentration phase $Bi_2VO_{5.5}$ [29]. In addition, a change in orientation was observed under different RF powers. This could be ascribed to changes in the Bi/V ratio in the films, which was also observed when we used the other target with different Bi/V ratios (Figure S4). Note that the crystallization process mainly occurs at the annealing period (Figure 4c). However, the mechanism of this phenomenon is unclear, and beyond the scope of this study. The Rietveld refinement method [30] was used to confirm the phase of the prepared films at 200 W. The obtained diffraction peaks were found to agree with the CIF data, and this pattern can be identified as a monoclinic scheelite structure [31]. As a result, the fitting demonstrates a desirable residual parameter in the Rietveld refinement (good of fitness = 2.3).

As shown in Figure 4d–f, the morphologies of the deposited $BiVO_4$ films under different RF powers were characterized by using SEM. All the films show grains, which indicates the polycrystalline structures. The grain sizes exhibit distinctive differences; the film deposited under 120 W expresses the smallest grain compared with other films, which may attribute to the excess Bi in the film. The films deposited under 50 W and 200 W show a 100–200 nm grain size, but the morphology is quite different. This can be connected to the XRD results of unique orientation.

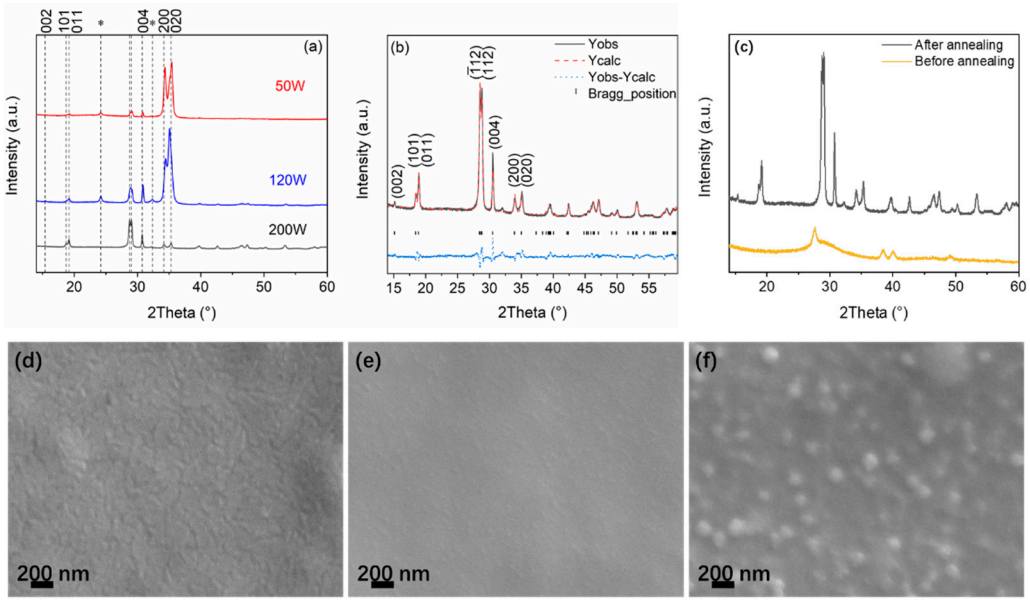

Figure 4. (**a**) XRD patterns of $BiVO_4$ films prepared under different RF powers; the impurity phase peaks are marked with asterisks (*). (**b**) Observed, calculated, and difference profiles of the Rietveld refinement for the sample prepared at 200 W. (**c**) XRD patterns of films prepared under 200 W before and after the annealing process. SEM images of $BiVO_4$ films deposited under (**d**) 50 W, (**e**) 120 W, and (**f**) 200 W.

3.6. PEC Measurement

The PEC performance of the bare monoclinic scheelite $BiVO_4$ film was investigated by linear sweep voltammetry (LSV) (Figure 5). The current density in the light-off state starts from approximately −0.08 V (vs. Ag/AgCl), which conforms to the standard electrode potential as follows:

$$S(s) + 2e^- \rightleftharpoons S^{2-} \quad E^0(V) = +0.14\ V. \tag{7}$$

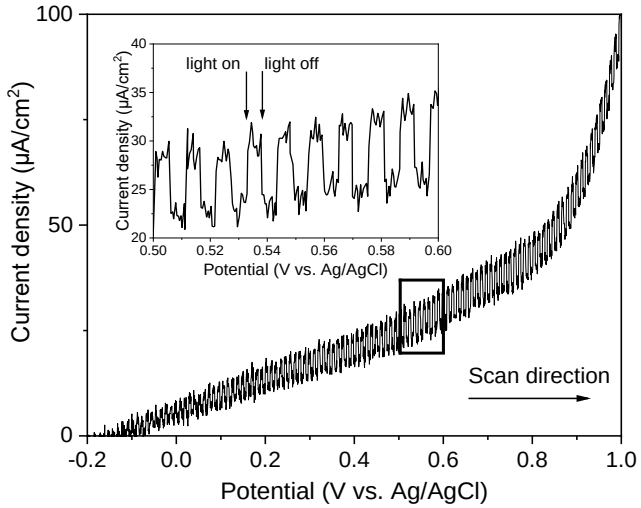

Figure 5. Chopped LSV of $BiVO_4$ film deposited on FTO at 200 W in an electrolyte containing 0.02 mol L^{-1} Na_2S and 0.02 mol L^{-1} Na_2SO_3 hole scavengers under simulated sunlight (AM 1.5G).

At the working anode, the electrons and holes are generated under the illumination of light. Then, the holes which can migrate to the surface of the $BiVO_4$ film will oxidize the S^{2-} ions in the solution. The generated electrons transferred by FTO layer to the cathode will participate in the reduction reaction on the Pt surface.

Under chopped illumination, the difference in the current density can be observed in the inset of Figure 5. The increased current density is provided by the extra electrons generated from the $BiVO_4$ film under visible-light illumination. The gain of photocurrent is at the level of $\mu A/cm^2$. Although the present performance cannot reach the level of films (~mA/cm^2) prepared using other mature methods [32], the performance is promising when the film thickness and crystal quality are optimized. Small photocurrents were also observed in thick films with thicknesses greater than 100 nm because of the short carrier diffusion length in $BiVO_4$ [33]. For this film, the lifetime of carriers was investigated by using time-resolved photoluminescence (Figure S5). The lifetime of carriers is around 0.87 ns, which is not enough for most photogenerated carriers to migrate to the surface. Therefore, improving the crystal quality and suppressing defects of the films is the next necessary work for obtaining high performance.

4. Conclusions

In summary, a monoclinic scheelite $BiVO_4$ film was successfully fabricated using the sputtering method at 200 W RF power from a compound $BiVO_4$ target. The Bi-richness of the films deposited at lower RF power has been attributed to the imbalanced sputtering yields of Bi and V atoms from the target and the diffusion in the target. For the other two processes, the simulation demonstrates that the atom transfer mechanism from the target to the substrate is different for the two types of atoms. The V atoms are easily scattered by the Ar background gas at a certain pressure, which results in less arrived V atoms on the substrate. Due to the difference in sublimation heat, the adsorbed number of Bi atoms drops faster than that of V atoms with increasing substrate temperature. Therefore, the ratio of Bi and V can also be finely controlled through these two processes. In this study, the appropriate ratio was reached at 200 W RF power, and the bare $BiVO_4$ film exhibited photocatalytic activity as a photoanode.

Supplementary Materials: The following are available online at https://www.mdpi.com/article/10.3390/en14082122/s1, Figures S1–S5. Figure S1, XPS spectra of the film before and after argon ion etching. The surface of the film exhibits the excess V after etching (according to the peak area), reflecting the preferential sputtering of Bi in the etching. Meanwhile, the metal state of Bi appears in the etched film, suggesting the oxygen was preferentially sputtered, too. The argon plasma was produced by the electric field of 300 V with the Ar pressure of 5×10^{-2} Pa, and etching time was 60 s. Figure S2, XPS spectra of the etched film at different temperatures in the vacuum (~5×10^{-5} Pa). The metal state of Bi gradually disappears with increasing temperature. At approximately 200 °C, the oxygen starts diffusing from bulk to surface. Until the temperature went up to 400 °C, the ratio of Bi and V changed. Therefore, the Bi diffused from bulk to surface. Figure S3, Raman spectra of films prepared at various substrate temperatures. With the increasing temperature, the Raman modes of V_2O_5 appear. It implies the different adsorbed amount of Bi and V on substrate resulting from temperature. Figure S4, XRD patterns of the prepared $BiVO_4$ films under different RF powers by using $BiV_{1.5}O_x$ target. Comparing with the structure of films prepared using $BiVO_4$ target, it can be demonstrated that the orientation changed from (020) to (112), which may be caused by increased vanadium in the films. Figure S5, TRPL decay of $BiVO_4$ films deposited under 200 W on the glass, collected at ~660 nm. The wavelength of excitation laser is 400 nm.

Author Contributions: Conceptualization, T.S.; data curation, J.L., K.T., and S.I.; formal analysis, I.A.; funding acquisition, M.M.I. and T.S.; investigation, J.L. and K.T.; supervision, T.S.; writing—original draft, J.L.; writing—review and editing, M.M.I. and T.S. All authors have read and agreed to the published version of the manuscript.

Funding: This work was supported by JSPS Grants-in-Aid for Scientific Research (KAKENHI), awards no. 19H02656, 18K05010, 19H02822, and 17F17385.

Institutional Review Board Statement: Not applicable.

Informed Consent Statement: Not applicable.

Data Availability Statement: Data is contained within the article and Supplementary Materials.

Acknowledgments: This work was supported by China Scholarship Council (CSC, 201907565031).

Conflicts of Interest: The authors declare no conflict of interest.

References

1. Lewis, N.S. Research opportunities to advance solar energy utilization. *Science* **2016**, *351*, aad1920. [CrossRef]
2. Chen, S.; Wang, L. Thermodynamic Oxidation and Reduction Potentials of Photocatalytic Semiconductors in Aqueous Solution. *Chem. Mater.* **2012**, *24*, 3659–3666. [CrossRef]
3. Tokunaga, S.; Kato, H.; Kudo, A. Selective Preparation of Monoclinic and Tetragonal $BiVO_4$ with Scheelite Structure and Their Photocatalytic Properties. *Chem. Mater.* **2001**, *13*, 4624–4628. [CrossRef]
4. Abdi, F.F.; Berglund, S.P. Recent developments in complex metal oxide photoelectrodes. *J. Phys. D Appl. Phys.* **2017**, *50*, 193002. [CrossRef]
5. Cooper, J.K.; Gul, S.; Toma, F.M.; Chen, L.; Glans, P.A.; Guo, J.; Ager, J.W.; Yano, J.; Sharp, I.D. Electronic Structure of Monoclinic BiVO4. *Chem. Mater.* **2014**, *26*, 5365–5373. [CrossRef]
6. Pihosh, Y.; Turkevych, I.; Mawatari, K.; Uemura, J.; Kazoe, Y. Photocatalytic generation of hydrogen by core-shell $WO_3/BiVO_4$ nanorods with ultimate water splitting efficiency. *Sci. Rep.* **2015**, 1–2. [CrossRef]
7. Dubal, D.P.; Jayaramulu, K.; Zboril, R.; Fischer, R.A.; Gomez-Romero, P. Unveiling $BiVO_4$ nanorods as a novel anode material for high performance lithium ion capacitors: Beyond intercalation strategies. *J. Mater. Chem. A* **2018**, *6*, 6096–6106. [CrossRef]
8. Coelho, D.; Gaudêncio, J.P.R.S.; Carminati, S.A.; Ribeiro, F.W.P.; Nogueira, A.F.; Mascaro, L.H. Bi electrodeposition on WO_3 photoanode to improve the photoactivity of the $WO_3/BiVO_4$ heterostructure to water splitting. *Chem. Eng. J.* **2020**, *399*, 125836. [CrossRef]
9. Wang, Y.; Shi, H.; Cui, K.; Zhang, L.; Ge, S.; Yu, J. Reversible electron storage in tandem photoelectrochemical cell for light driven unassisted overall water splitting. *Appl. Catal. B Environ.* **2020**, *275*, 119094. [CrossRef]
10. Park, Y.; McDonald, K.J.; Choi, K.S. Progress in bismuth vanadate photoanodes for use in solar water oxidation. *Chem. Soc. Rev.* **2013**, *42*, 2321–2337. [CrossRef]
11. Kang, D.; Kim, T.W.; Kubota, S.R.; Cardiel, A.C.; Cha, H.G.; Choi, K.S. Electrochemical Synthesis of Photoelectrodes and Catalysts for Use in Solar Water Splitting. *Chem. Rev.* **2015**, *115*, 12839–12887. [CrossRef] [PubMed]
12. Barranco, A.; Borras, A.; Gonzalez-Elipe, A.R.; Palmero, A. Perspectives on oblique angle deposition of thin films: From fundamentals to devices. *Prog. Mater. Sci.* **2016**, *76*, 59–153. [CrossRef]
13. Chen, L.; Alarcón-Lladó, E.; Hettick, M.; Sharp, I.D.; Lin, Y.; Javey, A.; Ager, J.W. Reactive Sputtering of Bismuth Vanadate Photoanodes for Solar Water Splitting. *J. Phys. Chem. C* **2013**, *117*, 21635–21642. [CrossRef]
14. Pedroni, M.; Chiarello, G.L.; Haghshenas, N.; Canetti, M.; Ripamonti, D.; Selli, E.; Vassallo, E. Bismuth vanadate photoanodes for water splitting deposited by radio frequency plasma reactive co-sputtering. *J. Vac. Sci. Technol. B* **2019**, *38*, 12203. [CrossRef]
15. Venkatesan, R.; Velumani, S.; Ordon, K.; Makowska-Janusik, M.; Corbel, G.; Kassiba, A. Nanostructured bismuth vanadate ($BiVO_4$) thin films for efficient visible light photocatalysis. *Mater. Chem. Phys.* **2018**, *205*, 325–333. [CrossRef]
16. Lamers, M.; Fiechter, S.; Friedrich, D.; Abdi, F.F.; van de Krol, R. Formation and suppression of defects during heat treatment of $BiVO_4$ photoanodes for solar water splitting. *J. Mater. Chem. A* **2018**, *6*, 18694–18700. [CrossRef]
17. Settaouti, A.; Settaouti, L. Simulation of the transport of sputtered atoms and effects of processing conditions. *Appl. Surf. Sci.* **2008**, *254*, 5750–5756. [CrossRef]
18. Nichols, M.T.; Li, W.; Pei, D.; Antonelli, G.A.; Lin, Q.; Banna, S.; Nishi, Y.; Shohet, J.L. Measurement of bandgap energies in low-k organosilicates. *J. Appl. Phys.* **2014**, *115*, 94105. [CrossRef]
19. Abrahamson, A.A. Born-Mayer-Type Interatomic Potential for Neutral Ground-State Atoms with Z = 2 to Z = 105. *Phys. Rev.* **1969**, *178*, 76–79. [CrossRef]
20. Ishida, M.; Yamaguchi, Y.; Yoshinaga, H.; Yamamura, Y. Dynamical simulation of sputtering and reflection from a ternary alloy. *Radiat. Eff. Defects Solids* **1997**, *142*, 287–299. [CrossRef]
21. Berg, S.; Katardjiev, I.V. Preferential sputtering effects in thin film processing. *J. Vac. Sci. Technol. A* **1999**, *17*, 1916–1925. [CrossRef]
22. Carter, G.; Katardjiev, I.V.; Nobes, M.J. An altered layer model for sputter-profiling. *Surf. Interface Anal.* **1989**, *14*, 194–208. [CrossRef]
23. Seah, M.P.; Clifford, C.A.; Green, F.M.; Gilmore, I.S. An accurate semi-empirical equation for sputtering yields I: For argon ions. *Surf. Interface Anal.* **2005**, *37*, 444–458. [CrossRef]
24. Dam, B.; Rector, J.H.; Johansson, J.; Huijbregtse, J.; De Groot, D.G. Mechanism of incongruent ablation of $SrTiO_3$. *J. Appl. Phys.* **1998**, *83*, 3386–3389. [CrossRef]
25. Wasa, K.; Hayakawa, S. *Handbook of Sputter Deposition Technology*; Noyes Publications: Park Ridge, NJ, USA, 1992; pp. 78–84, ISBN 0-8155-1280-5.
26. Asnin, L.D.; Chekryshkin, Y.S.; Fedorov, A.A. Calculation of the sticking coefficient in the case of the linear adsorption isotherm. *Russ. Chem. Bull.* **2003**, *52*, 2747–2749. [CrossRef]
27. De Boer, J.H. *Adsorption Phenomena*; Frankenburg, W.G., Komarewsky, V.I., Rideal, E.K., Eds.; Academic Press: Cambridge, MA, USA, 1956; Volume 8, pp. 85–92. ISBN 0360-0564.
28. Kölbach, M.; Harbauer, K.; Ellmer, K.; van de Krol, R. Elucidating the Pulsed Laser Deposition Process of $BiVO_4$ Photoelectrodes for Solar Water Splitting. *J. Phys. Chem. C* **2020**, *124*, 4438–4447. [CrossRef]

29. Gong, H.; Freudenberg, N.; Nie, M.; van de Krol, R.; Ellmer, K. $BiVO_4$ photoanodes for water splitting with high injection efficiency, deposited by reactive magnetron co-sputtering. *AIP Adv.* **2016**, *6*, 45108. [CrossRef]
30. Rietveld, H.M. Line profiles of neutron powder-diffraction peaks for structure refinement. *Acta Crystallogr.* **1967**, *22*, 151–152. [CrossRef]
31. Sleight, A.W.; Chen, H.; Ferretti, A.; Cox, D. Crystal growth and structure of $BiVO_4$ Locality: Synthetic Sample: T = 295 K. *Mater. Res. Bull.* **1979**, *14*, 1571–1581. [CrossRef]
32. Abdi, F.F.; Firet, N.; van de Krol, R. Efficient $BiVO_4$ Thin Film Photoanodes Modified with Cobalt Phosphate Catalyst and W-doping. *ChemCatChem* **2013**, *5*, 490–496. [CrossRef]
33. Rettie, A.J.E.; Mozaffari, S.; McDaniel, M.D.; Pearson, K.N.; Ekerdt, J.G.; Markert, J.T.; Mullins, C.B. Pulsed Laser Deposition of Epitaxial and Polycrystalline Bismuth Vanadate Thin Films. *J. Phys. Chem. C* **2014**, *118*, 26543–26550. [CrossRef]